*Received:* 28 December 2023 | *Revised:* 2 March 2024 | *Accepted:* 3 April 2024
*DOI: 10.37917/ijeee.22.1.9* *Vol. 22 | Issue 1 | June 2026*

Iraqi Journal for Electrical and Electronic Engineering
*Original Article*

Open Access
IJEEE University of Basrah College of Engineering

# Detection of Lumbar Spine Stenosis in MRI Spinal Imaging

**Mohammed A. Abed[1], Z.T.Al-Qaysi *[1], Aws Q.Hamdi[2], Salwa K.Abdulateef[1], M.A.Ahmed[1], Mahmood M. Salih[1]**
[1] Department of Computer Science, Computer Science and Mathematics College, Tikrit University, Tikrit, Iraq
[2]Department of Radiology, College of Medicine, Tikrit University, Tikrit, Iraq

Correspondance
*Z.T.Al-Qaysi
Department of Radiology, College of Medicine,
Tikrit University, Tikrit, Iraq
Email: ziadoontareq@tu.edu.iq

**Abstract**
***Lumbar spine stenosis (LSS) is a common reason for low back pain, which refers to anatomical spinal canal stenosis. It often causes pressure on the nerve elements due to the surrounding soft tissue and bone. Due to the huge number of spinal injuries, manual diagnosis of lumbar spine stenosis by radiologists is tedious or time-consuming. Therefore, Deep learning techniques have become a more helpful tool to overcome this problem. For this purpose, this study employed the YOLO-v5 to develop an LSS detection model on a dataset of lumbar spine MRI scans from 153 patients with symptomatic low back pain. The dataset was filtered to include 84 mid-sagittal images using annotation techniques. The detection model is utilized to classify the intervertebral disc (IVD) condition as either bulging or normal. The results obtained showed that the model achieved an accuracy exceeding 88% in detecting and classifying the lumbar spine vertebra. The developed models showed that they are effective for lumbar intervertebral disc classification.***

**Keywords**
**Lumbar Spine, Stenosis, Intervertebral Disc, MRI Image, Bulging Disc, Deep Learning, YOLO-v5.**

## I. Introduction

The spine serves as the central support structure of the human body, with the lumbar spine being the primary source of human physical power. Consequently, diseases affecting the lumbar spine commonly arise in the course of daily activities and work for individuals. Hence, comprehending the composition of the lumbar intervertebral disc and interpreting the MRI scans of the lumbar and intervertebral discs is crucial for getting a comprehensive understanding of individuals' health [1]. The lumbar spine is the lower portion of the spinal column, which is located beneath the last thoracic vertebra (T12) and the first sacral vertebra (S1). In this region, the spinal cord is protected by five strong and movable vertebrae (L1-L5), which help to distribute the forces acting on the spine [2]. Fig. 1 shows the MRI anatomy classification of the Lumbar spine.

Lower back pain can indeed be caused by a variety of conditions, including the loss of height of one or more intervertebral discs (IVDs) [3]. The lumbar intervertebral disc (IVD) is a fully integrated and functional structural component, comprising the annulus fibrosus and nucleus pulposus. Lumbar IVD is susceptible to degenerative changes or lumbar spine stenosis (LSS) as a result of physiological and pathological factors [4]. LSS is a common cause of lumbar surgery, which refers to anatomical stenosis of the spinal canal, and It often causes pressure on the nerve elements due to the surrounding soft tissue and bone [5]. Disc bulging is a common problem of lumbar spine stenosis includes anterior and posterior disc bulging, which was measured as the area of the disc portion that exceeded the anterior or posterior edges of vertebral bodies [6]. Fig. 2 shows the MRI image of normal and bulging disc. Magnetic resonance imaging (MRI) has become a more efficient way to diagnose lumbar spine stenosis; MRI provides detailed images of nerves and discs, which help in the diagnosis of LSS, as well as providing a dataset

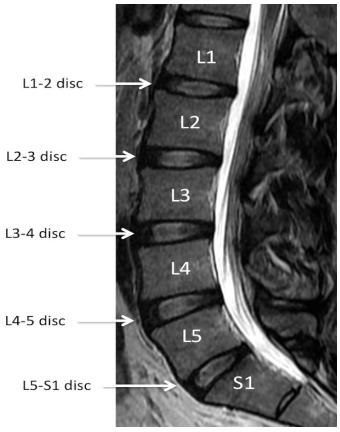


Fig. 1. Lumbar Spine MRI Vertebrae Classification.

for training a deep learning (DL) model [7]. The DL technique is used to classify medical images and signals. These techniques have yielded encouraging outcomes through the utilization of complex network architectures [8]. By establishing a DL model, diseases can be automatically located and detected using object detection techniques in patient diagnosis systems [9].

Object detection based on YOLO techniques has been an active area of research in the medical field for cancer detection, skin segmentation, pill identification, and lumbar spine stenosis detection, leading to improved diagnostic accuracy and treatment which is a more efficient process [10]. YOLO is well-known for its object detection capabilities, which are characterized by their exceptional speed. This is because YOLO only requires inputting the image into the network to obtain the final detection result [11]. YOLO-v5, which is an enhanced version of YOLO-v4, has several advantages such as high speed, ease of use, and good accuracy; therefore, it has been utilized in this study for LSS detection [12].

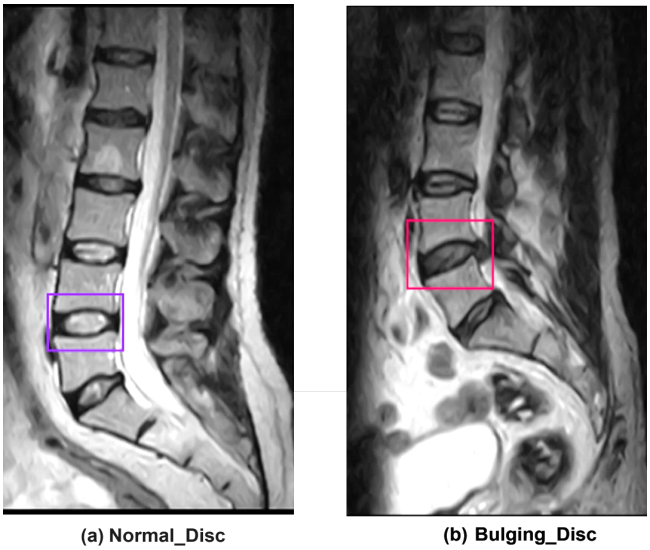


Fig. 2. e.g. MRI image of Normal and Bulging disc.

According to the above, an LSS detection deep learning model has been developed in this study using YOLOv5 with lumber spine MRI dataset for identifying the status of IVD normal or bulging. The following is the structure of the reminder for this paper: data collection, data preprocessing, and model evaluation performance defined in sec. II. , experimental results presented in sec. III. , and discussion and findings presented in sec. IV. .

## II. Materials and Methods

### A. LSS Detection Model Implementation

Fig. 3 outlines the primary and comprehensive steps involved in implementing the LSS detection model, making the process easier to understand. There are three primary steps in the process:

1. Data preparation: To create the dataset needed for training, assessing, and testing the YOLO model, MRI images are gathered, pre-processed, filtered, and annotated.
2. Model implementation: This process involves choosing a deep learning model, training it on the training and validation datasets, and assessing it on the test dataset.
3. Model inference: The detection model is applied to new MRI LSS images to validate the developed model.

### B. Data Collection

The dataset was obtained from Al-Tawfiq Private Hospital for Surgical Specialties after obtaining all necessary and ethical approvals. The dataset includes normal and abnormal cases. Fig. 4 shows different sample dataset images. It contains MRI images of 153 patients (5355 images) of different ages and genders suffering from lumbar spine stenosis, each with a size of 448 × 448. The data was collected by a Hitachi Airis II 0.3 Tesla Open MRI scanner using a special MRI lumbar spine protocol T1 and T2 weight of sagittal and axial views. Our study takes images of the T2 weight of the sagittal view of the lumbar spine. MRI imaging parameters are key settings that determine the characteristics of the acquired images. These parameters play a crucial role in tailoring MRI scans to specific clinical needs and desired imaging outcomes, and they are different from one device to another. The most effective parameter values used during traverse MRI scans are provided in Table I. The parameters set for the MRI protocol that has been used for the data acquisition in this study are explained as follows:

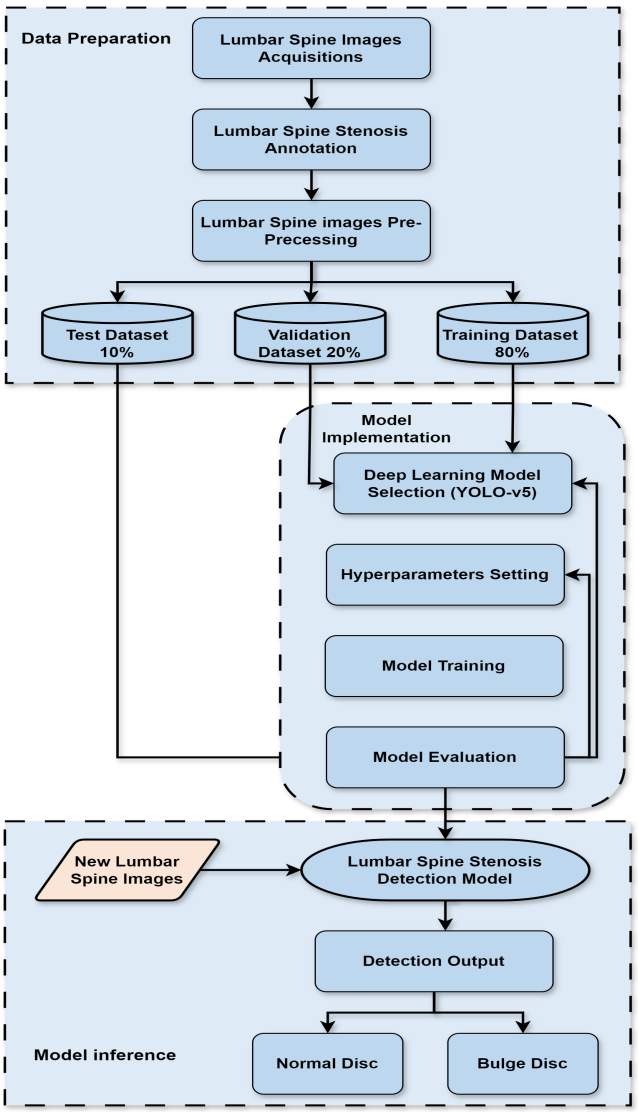


Fig. 3. Methodological framework for the LSS Detection Model.

Fig. 4. Sample Lumbar Spine Images from Dataset.

1. TR (Repetition Time): TR refers to the interval of time between consecutive pulse sequences or repetitions. The unit of measurement is milliseconds (ms). A longer TR can increase the signal intensity and is often used in sequences where T1 weighting is desired [13].

2. TE (Echo Time): TE refers to the duration from when the radiofrequency pulse is applied to when the signal echo reaches its highest point. The unit of measurement is milliseconds (ms). Short TE values are associated with T1-weighted images, while longer TE values are associated with T2-weighted images [14].

3. NEX (Number of Excitations): NEX represents the number of signal averages. Increasing NEX improves signal-to-noise ratio (SNR) but prolongs scan time [15].

4. Slice Thickness: Slice thickness refers to the thickness of each imaging slice and is typically measured in millimeters (mm). Thinner slices provide higher resolution but may increase scan time [16].

5. FOV (Field of View): FOV refers to the physical dimensions of the imaging area and is typically quantified in millimeters. It determines how much anatomy is covered in each image. A larger FOV captures more anatomy but may result in lower resolution [17].

6. Matrix: The matrix represents the total number of pixels in both the rows and columns of the image. Larger matrix sizes result in higher spatial resolution but may increase data acquisition time and storage requirements [18].

TABLE I.
THE RANGE OF ACQUISITION PARAMETER VALUES USED DURING MRI SCANS.

| Sequence Type | T2 -weighted |
|---|---|
| TR (Repetition Time) | 3000 ms |
| TE (Echo Time) | 120 ms |
| Slice Thickness | 6.0 mm |
| FOV (Field of View) | 350 mm |
| Matrix (Freq. x Phase) | 256 × 168 |
| NEX (Number of Excitation) | 6 |

### *C. Data Pre-Processing*

Fundamentally, with the assistance of the radiologist, the dataset was filtered, annotated, and classified. The process of filtering and labeling the data includes the following steps:

1. Exclude noise, artifacts, and outside conditions in spinal stenosis cases.
2. Our work is divided into two classes: normal and bulging discs, and excludes other lumbar spine stenosis cases as shown in Fig. 5.
3. It has manually labeled (polygon annotation) the mid-sagittal lumbar spine image chosen at the anatomical level of the intervertebral disc between L4 and L5 (the vertebra that is more susceptible to spinal stenosis because of its unique anatomy and function).
4. Use the Radiant Dicom viewer software. It supports multiple DICOM file types and can open and display studies obtained from different imaging modalities.
5. We are exporting the mid-sagittal image (optimal view to visualize the spinal cord) from patient data of the T2 weight of the lumbar spine in jpeg image format with a resolution of 1920 × 1080 px, as shown in Fig. 6.
6. Stretch the image size to 640 × 640 to prepare it for training using the YOLO-V5 models.
7. Color System → Gray Scale.
8. Horizontal crop 15 %.

For more details on how to extract images from patients' data, Fig. 7 explains more details about choosing and balancing the data between normal and bulging discs.

### *D. Model Training*

Python 3.6 was employed in the model's development. Google Colaboratory was used to train and validate the algorithms. The deep learning approach employed the deep convolutional

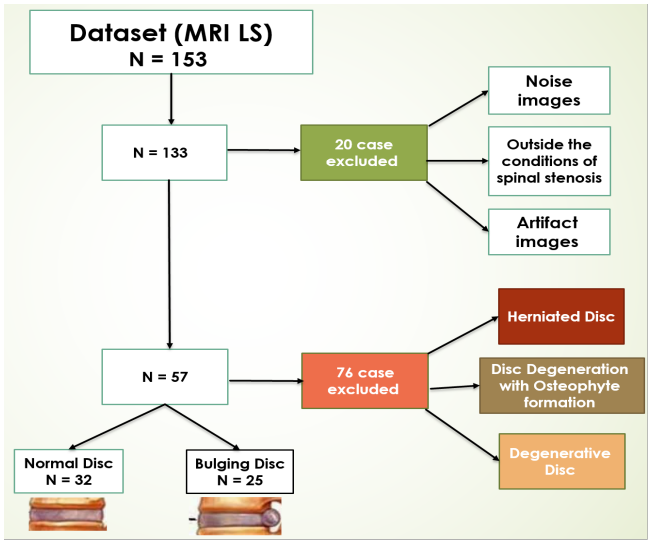


Fig. 5. Systematic Review of Dataset Filtering.

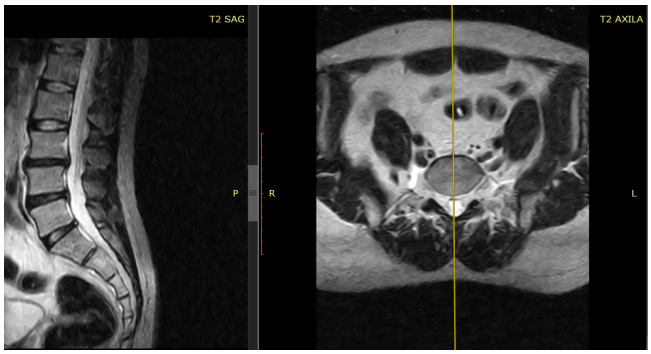


Fig. 6. Mid-Sagittal image for Lumbar spine.

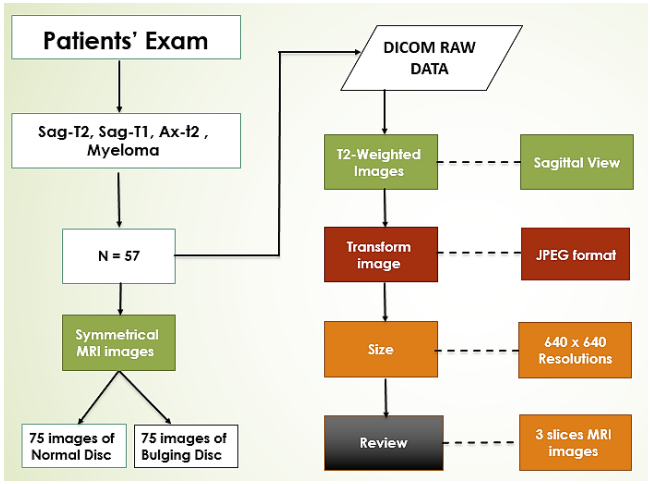


Fig. 7. Process flow of data processing.

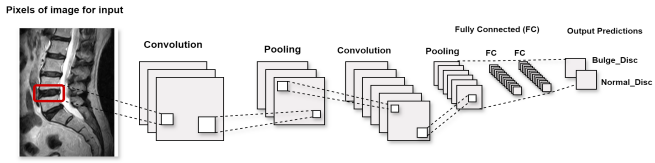


Fig. 8. Deep learning architecture model used convolutional neural network (CNN).

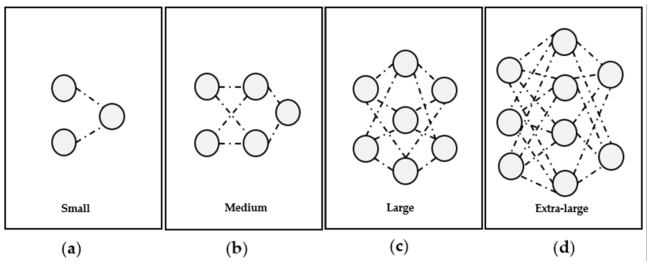


Fig. 9. YOLOv5 architectural size: Small-YOLOv5s (a), Medium-YOLOv5m (b), Large-YOLOv5l (c), and (d) Extra-large-YOLOv5x.

neural network (CNN) model to train, detect, and classify intervertebral disc degeneration (IDD) as shown in Fig. 8. Nevertheless, this version cannot determine the phase of the backbone pictures. In this study, it was employed the YOLOv5 architecture that is shown in Fig. 9 for efficient object detection. This architecture partitions an image into a grid system, with each grid module responsible for detecting objects within its boundaries. A total of 100 epochs and batch size 16 have been performed to test each version. Fig. 10 shows the architecture of YOLO-v5 used for the detection of LSS. The final dataset after the filtering process included 84 images of sagittal T2 weight divided into three groups and was randomly

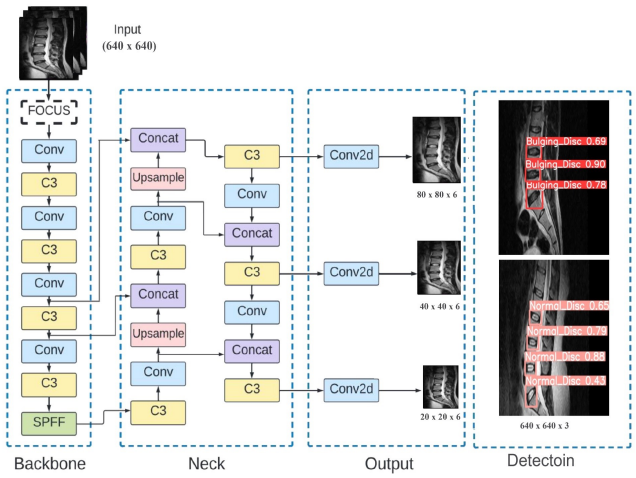


Fig. 10. The general architecture of YOLO-v5

split into an internal training set (70 %), validation set (20 %), and test set (10 %).

### *E. Model Performance Evaluation Metrics*

The model detection was evaluated using accuracy, F1 score, recall, precision, train and validation box loss, obj loss, class loss, and mean average precision. The evaluation metrics that were used to evaluate the model performance are explained as follows:

Precision: Precision is a measure of a network's ability to identify targets at a single threshold accurately, calculated by:

$$\text{precision} = \frac{\text{true positive}}{\text{actual positive}} \quad \text{or} \quad \frac{\text{TP}}{\text{TP}+\text{FP}} \tag{1}$$

Recall is a measure of the network's ability to detect its target, calculated by:

$$\text{recall} = \frac{\text{true positive}}{\text{predicted results}} \quad \text{or} \quad \frac{\text{TP}}{\text{TP}+\text{FN}} \tag{2}$$

The F1-score metric is used as a singular measure to assess the accuracy of our models. The F1-score is a composite metric that combines the Precision and Recall measures, effectively balancing both precision and recall. It serves as a single metric that accurately represents the overall performance of the model.

$$\text{F1} = 2 \times \frac{\text{Precision} \times \text{recall}}{\text{Precision} + \text{recall}} \tag{3}$$

The Intersection over Union (IoU) is computed by dividing the area of overlap between two boxes by the total area covered by both boxes. In other words, it measures the model's ability to differentiate between objects and their backgrounds in an image. Fig. 11 shows a diagrammatic representation of IoU.

$$\text{IoU} = \frac{\text{TP}}{\text{TP}+\text{FN}+\text{FP}} \tag{4}$$

The Average Precision (AP), also known as Mean Average Precision (mAP), is a widely used metric for assessing the performance of object detection models.

$$\text{mAP} = \frac{1}{n}\sum_{i=1}^{n} \text{AP}i \tag{5}$$

The training loss represents the cost of inaccurate predictions, calculated by measuring the discrepancy between the predicted and actual values. There exist three categories of losses:

- The box loss measures the difference between the predicted bounding boxes and the true bounding boxes of the objects present in the training data.

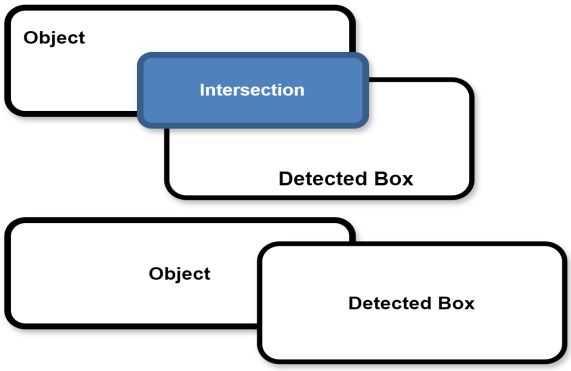


Fig. 11. e.g. intersection over union calculation

- The object loss refers to the difference in the presence of objects within each grid. High objectivity indicates a high likelihood of an object being present in the image window.
- The classification loss measures the difference in class assignment between the target and detected objects.

The evaluation metrics are computed using the formula mentioned previously, taking into account the following conditions [19]:

- TP (True Positive): The number of instances that were correctly predicted as positive.
- TN (True Negative): The number of instances that were correctly predicted as negative.
- FP (False Positive): The number of instances that were incorrectly predicted as positive.
- FN (False Negative): The number of instances that were incorrectly predicted as negative.

## III. Results

This section describes the result of the LSS detection model using yolov5 models. Basically, there are several models for Yolov5, including: (a) Yolo-v5s, (b) Yolo-v5m, (c) Yolo-v5l, (d) and Yolo-v5x. The result of these models is shown in Fig. 12 and Fig. 13. More details are described in the following subsections: The YOLO-v5 model incorporates box losses in its object detection algorithm to enhance the accuracy of object detection and classification within an image. The goal during training is to minimize the losses to the lowest possible value. The precision and recall values approached unity, indicating excellent performance. The mean average precision, the most commonly used statistic, also met expectations. Fig. 14 shows the training box loss of the dataset. Fig. 15 displays

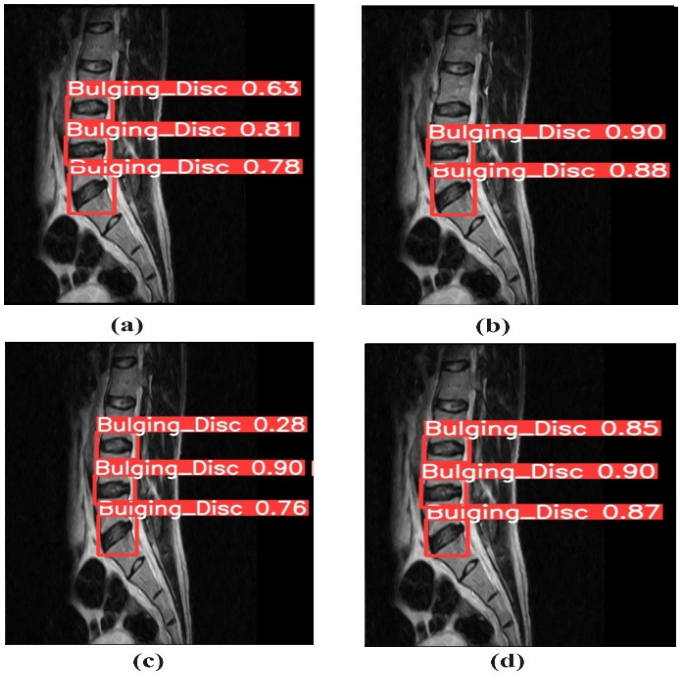


Fig. 12. Result of bulging disc detection using different YOLO-v5 models (a) YOLO -v5s, (b) YOLO -v5m, (c) YOLO -v5l, (d) YOLO -v5x.

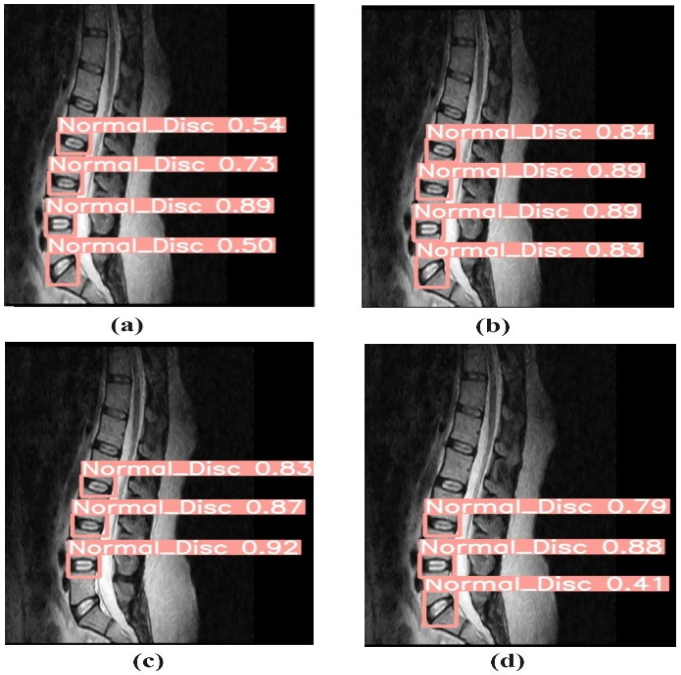


Fig. 13. Result of Normal disc detection using different YOLO-v5 models (a) YOLO-v5s, (b) YOLO-v5m, (c) YOLO-v5l, (d) YOLO-v5x.

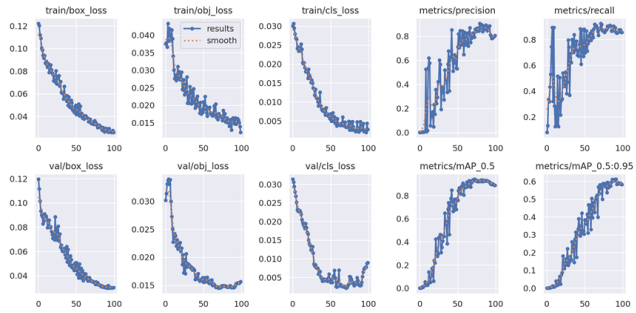


Fig. 14. Performance training analysis with a large YOLO-v5 model.

the confusion matrix of the YOLO-v5l model, which was used to analyze the accuracy of the collected data in determining the status of LSS.

The light blue background signifies the presence of true negative values. The true negative values represent the instances where the model accurately predicted the negative class when the actual class was indeed negative. The bulging disc has a measurement of 1.00, while the normal disc has a measurement of 0.82. Fig. 16 displays the F1 scores corresponding to the confidence values. The provided figure displays the F1 scores for disc bulging and normal conditions. The highest score achieved by the LSS detection model is 0.87, with a confidence level of 0.521. Fig. 17 displays the Precision-Recall Curve, with a specific region in the lower left utilized for calculating the Average Precision (AP) score for the LSS detection model. The graph in Fig. 18 displays the relationship between precision and confidence. A confidence level greater than 0.756 indicates satisfactory precision in the scores which is considered good for the developed LSS detection model. The relationship between the confidence and recall values is analogous to that shown in Fig. 19. Table II shows the computational time for each YOLO-v5 model with 100 epoch training. Table III shows a comparison of the LSS

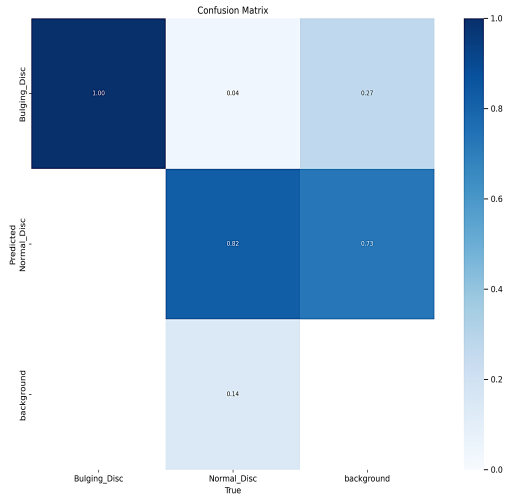


Fig. 15. displays a confusion matrix that represents the training model's accuracy.

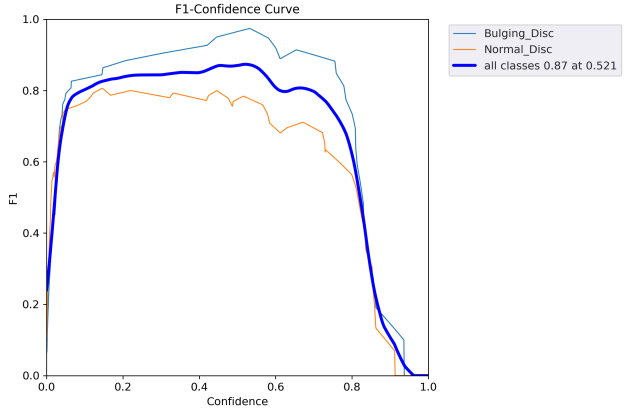


Fig. 16. illustrates the correlation between the F1 score and the confidence curve.

TABLE II.
RESULTS OF COMPUTATIONAL TIME OF YOLO-V5 MODELS

| Model | Computational time |
|---|---|
| YOLO-V5n | 0.080 hours |
| YOLO-V5s | 0.113 hours |
| YOLO-V5m | 0.188 hours |
| YOLO-V5L | 0.294 hours |
| YOLO-V5X | 0.577 hours |

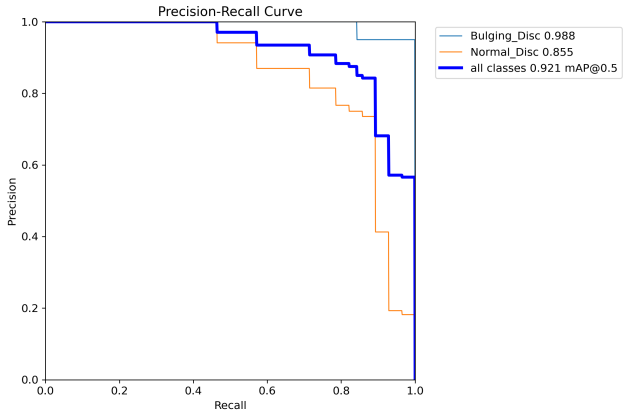


Fig. 17. displays a graph illustrating the correlation between recall and precision.

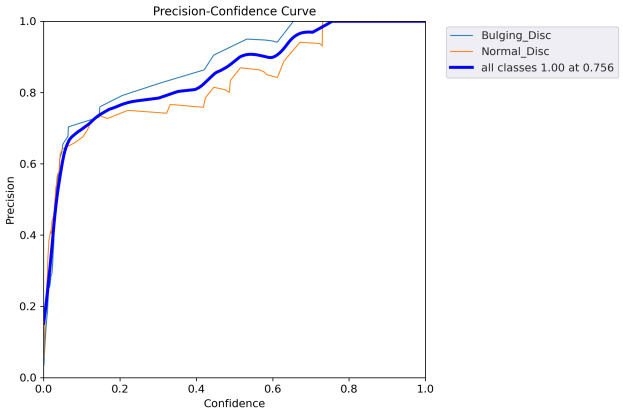


Fig. 18. displays a graph illustrating the correlation between precision and confidence.

detection results between YOLO5 models.

TABLE III.
RESULTS OF YOLO-V5 MODELS

| Model | mAP 0.5 | precision | Recall | F1-Score |
|---|---|---|---|---|
| YOLO-V5n | 89 % | 88 % | 80 % | 82 % |
| YOLO-V5s | 89 % | 81 % | 87 % | 85 % |
| YOLO-V5m | 90 % | 80 % | 94 % | 87 % |
| YOLO-V5L | 92 % | 88 % | 86 % | 87 % |
| YOLO-V5X | 90 % | 89 % | 83 % | 86 % |

## IV. DISCUSSION

Fundamentally, for the LSS detection models, the F1 curve revealed that the confidence value that maximized both precision and recall is 0.521. In numerous instances, a greater confidence value is preferable. For this particular model, it is advisable to choose a confidence level of 0.6, as the F1 score was approximately 0.87 and it is different from one model to another of YOLO-v5. Fig. 10 and Fig. 11 shows the results of the prediction using different YOLO-v5 models on the same patient images. In Fig. 10 the better result was in the model (c) YOLO-v5L to detect the bulging disc, while in Fig. 11 the better result was in (b) model to detect the normal disc. YOLO-v5 models differ in their depth and width parameters, but they follow the same architecture with three heads. Prisilla, A.A., et al [20], with a public dataset with 515 images (with augmentation) of sagittal view (5 slices) selected from different patients used different approaches of YOLO versions to diagnose lumbar spine herniates. The training dataset was combined with the radiologist's labeling and annotation. The results show Approximately 89 % of mAP.

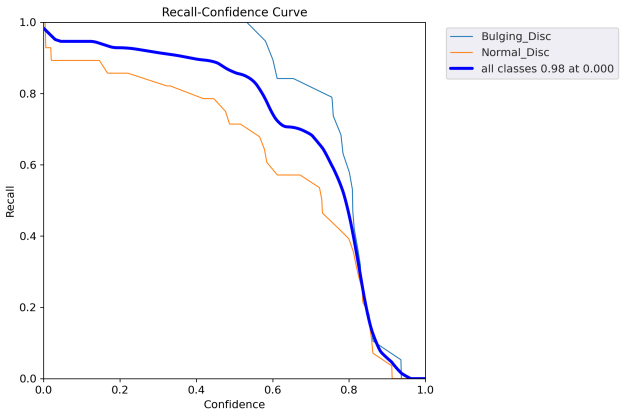


Fig. 19. displays a graph illustrating the correlation between the F1 score and confidence curves.

Sai JY, et al [21], used YOLO-v3 for automatic detection to assist the initial Lumbar disc herniation exam for lower back pain; the subjects were between 20 and 65 years old. The training dataset labeling and annotation with radiologists. The result of mean average precision (mAP) was 92.4 % at 550 images with data augmentation of sagittal view. Liawrungrueang W, et all [22], used YOLO-v5 to diagnose the lumbar spine status according to the Pfirrmann grading system using a public dataset. The training dataset labeling and annotation with radiologists. The result of mean average precision (mAP) was 92.4 % at 550 with data augmentation of sagittal view.

G. Valarmathi, et al [23], used a hyperactive classifier (YOLO-v2 and EGG16) for automatic localization and classification of intervertebral disc herniation. The proposed method is trained and validated using a real-world spine MRI image dataset obtained from a hospital. The results reveal that the proposed approach attains a high accuracy of 93.59 % for herniation detection, comfortably outperforming other state-of-the-art methodologies. From the above-related studies, auto detection and classification of the LSS of IVD is not always accurate. In the present study, we focus on three important factors regardless of accuracy:

- First: type of MRI scanner device (open or closed).
- Second: values of parameters used in MRI protocol as in Table I.
- Third: meeting with the radiologist to identify (manual labeling) the IVD status as normal or bulging and which images of patients' data are suitable for model training.

The first and second factors above affect image quality, which holds significant importance in the context of deep learning algorithms. As a result, it is not possible to generalize the data to all patients.

TABLE IV.
THE CONTRIBUTION OF OUR STUDY IN CONTRAST TO PREVIOUS STUDIES

| Author's name | 2026 of publication | method | Dataset (private, public) | Data annotation of lumbar spine vertebra (sag-view) | Scanner device type (open, closed) | Parameters of MRI protocol for acquisition images |
|---|---|---|---|---|---|---|
| Our study | - | Yolo-v5 | Private | L4-L5 | Open | Identified |
| Prisilla, A. A., et al. | 2023 | Yolo-v5, 6, 7 | Public | L1 to S1 | Closed | Not identified |
| Tsai JY, Hung IY, Guo YL, et al. | 2021 | Yolo-v3 | Private | L1 to S1 | Closed | Not identified |
| Liawrungrueang W, Kim P, et al. | 2023 | Yolo-v5 | Private | L1 to S1 | Closed | Not identified |
| G. Valarmathi and S. Nirmala Devi | 2023 | Yolo-v2_EVGG16 | Private | Auto localization | Closed | Not identified |

Table IV shows the contribution of our study in contrast to previous studies.

## V. CONCLUSION

Object detection based on YOLO techniques has been an active area of research in the medical field of lumbar spine stenosis detection, leading to improved diagnostic accuracy and treatment which is a more efficient process. Considering many versions of YOLO algorithms taking into account their accuracy, speed, and model size. Thus, this study adopted YOLO-v5, which is an enhanced version of YOLO-v4 and has several advantages such as high speed, ease of use, and good accuracy, to detect and grade the status of IVD as a normal or bulging disc. The experimental part of this study tested all the YOLO-v5 versions and the results showed that the YOLOv5L model exhibited a detection accuracy of over 88 % for lumbar intervertebral discs (IVD). They are effective for lumbar intervertebral disc degenerative change diagnoses. For future research, this study recommends train and testing the LSS detection model using a large dataset acquired from different sources of MRI devices.

## CONFLICT OF INTEREST

The authors have no conflict of relevant interest to this article.

## REFERENCES

[1] M. Han, E. Bahroos, M. E. Hess, C. T. Chin, K. T. Gao, D. D. Shin, J. E. Villanueva-Meyer, T. M. Link, V. Pedoia, and S. Majumdar, "Technology and tool development for BACPAC: Qualitative and quantitative analysis of accelerated lumbar spine MRI with deep-learning based image reconstruction at 3T," *Pain Medicine*, vol. 24, no. Suppl 1, pp. S149–S159, 2023.

[2] B. Sassack and J. D. Carrier., "Anatomy, back, lumbar spine," Aug. 2023. [Updated 2023 Aug 14]. In: StatPearls [Internet]. Treasure Island (FL): StatPearls Publishing; 2024 Jan.

[3] W. Mbarki, M. Bouchouicha, S. Frizzi, F. Tshibasu, L. B. Farhat, and M. Sayadi, "Lumbar spine discs classification based on deep convolutional neural networks using axial view MRI," *Interdisciplinary Neurosurgery*, vol. 22, p. 100837, 2020.

[4] M. Han, L. Liu, M. Hu, G. Liu, and P. Li, "Medical expert and machine learning analysis of lumbar disc herniation based on magnetic resonance imaging," *Computer Methods and Programs in Biomedicine*, vol. 213, p. 106498, 2022.

[5] Q. Li, Z. Du, and H. Yu, "Precise laminae segmentation based on neural network for robot-assisted decompressive laminectomy," *Computer methods and programs in biomedicine*, vol. 209, p. 106333, 2021.

[6] L. Chen, M. C. Battié, Y. Yuan, G. Yang, Z. Chen, and Y. Wang, "Lumbar vertebral endplate defects on magnetic resonance images: prevalence, distribution patterns, and associations with back pain," *The Spine Journal*, vol. 20, no. 3, pp. 352–360, 2020.

[7] N. C. Lehnen, R. Haase, J. Faber, T. Rüber, H. Vatter, A. Radbruch, and F. C. Schmeel, "Detection of degenerative changes on MR images of the lumbar spine with a convolutional neural network: a feasibility study," *Diagnostics*, vol. 11, no. 5, p. 902, 2021.

[8] U. Raghavendra, N. S. Bhat, A. Gudigar, and U. R. Acharya, "Automated system for the detection of thoracolumbar fractures using a CNN architecture," *Future Generation Computer Systems*, vol. 85, pp. 184–189, 2018.

[9] S. Wang, Y. Zha, W. Li, Q. Wu, X. Li, M. Niu, M. Wang, X. Qiu, H. Li, H. Yu, *et al.*, "A fully automatic deep learning system for COVID-19 diagnostic and prognostic analysis," *European Respiratory Journal*, vol. 56, no. 2, 2020.

[10] J. Terven, D.-M. Córdova-Esparza, and J.-A. Romero-González, "A comprehensive review of yolo architectures in computer vision: From yolov1 to yolov8 and yolo-nas," *Machine Learning and Knowledge Extraction*, vol. 5, no. 4, pp. 1680–1716, 2023.

[11] P. Jiang, D. Ergu, F. Liu, Y. Cai, and B. Ma, "A review of yolo algorithm developments," *Procedia computer science*, vol. 199, pp. 1066–1073, 2022.

[12] T. Diwan, G. Anirudh, and J. V. Tembhurne, "Object detection using YOLO: Challenges, architectural succes-

sors, datasets and applications," *multimedia Tools and Applications*, vol. 82, no. 6, pp. 9243–9275, 2023.

[13] S. Larmour, K. Chow, P. Kellman, and R. B. Thompson, "Characterization of T1 bias in skeletal muscle from fat in MOLLI and SASHA pulse sequences: quantitative fat-fraction imaging with T1 mapping," *Magnetic Resonance in Medicine*, vol. 77, no. 1, pp. 237–249, 2017.

[14] Y.-J. Ma, S. Jerban, H. Jang, E. Y. Chang, and J. Du, "Fat suppression for ultrashort echo time imaging using a novel soft-hard composite radiofrequency pulse," *Magnetic resonance in medicine*, vol. 82, no. 6, pp. 2178–2187, 2019.

[15] H. Kang, D. Noh, S.-K. Lee, S. Choi, and K. Lee, "Deep learning-based reconstruction can improve canine thoracolumbar magnetic resonance image quality and reduce slice thickness," *Veterinary Radiology & Ultrasound*, vol. 64, no. 6, pp. 1063–1070, 2023.

[16] V. M. Runge and J. T. Heverhagen, "3D imaging: basic principles," in *The Physics of Clinical MR Taught Through Images*, pp. 108–109, Springer, 2022.

[17] T. Kaasalainen, M. Ekholm, T. Siiskonen, and M. Kortesniemi, "Dental cone beam CT: An updated review," *Physica Medica*, vol. 88, pp. 193–217, 2021.

[18] M. Strzelecki, A. Piórkowski, and R. Obuchowicz, "Effect of matrix size reduction on textural information in clinical magnetic resonance imaging," *Journal of Clinical Medicine*, vol. 11, no. 9, p. 2526, 2022.

[19] R. P. Neelakandan, R. Kandasamy, B. Subbiyan, and M. A. Bennet, "Early detection of alzheimer's disease: An extensive review of advancements in machine learning mechanisms using an ensemble and deep learning technique," *Engineering Proceedings*, vol. 59, no. 1, p. 10, 2023.

[20] A. A. Prisilla, Y. L. Guo, Y.-K. Jan, C.-Y. Lin, F.-Y. Lin, B.-Y. Liau, J.-Y. Tsai, P. Ardhianto, Y. Pusparani, and C.-W. Lung, "An approach to the diagnosis of lumbar disc herniation using deep learning models," *Frontiers in Bioengineering and Biotechnology*, vol. 11, p. 1247112, 2023.

[21] J.-Y. Tsai, I. Y.-J. Hung, Y. L. Guo, Y.-K. Jan, C.-Y. Lin, T. T.-F. Shih, B.-B. Chen, and C.-W. Lung, "Lumbar disc herniation automatic detection in magnetic resonance imaging based on deep learning," *Frontiers in Bioengineering and Biotechnology*, vol. 9, p. 708137, 2021.

[22] W. Liawrungrueang, P. Kim, V. Kotheeranurak, K. Jitpakdee, and P. Sarasombath, "Automatic detection, classification, and grading of lumbar intervertebral disc degeneration using an artificial neural network model," *Diagnostics*, vol. 13, no. 4, p. 663, 2023.

[23] G. Valarmathi and S. N. Devi, "Automatic localization and classification of intervertebral disc herniation using hybrid classifier," *Biomedical Signal Processing and Control*, vol. 86, p. 105291, 2023.